The Crystal Structure of Exfoliative Toxin B: A Superantigen with Enzymatic Activity[†,‡]

Gregory M. Vath,[§] Cathleen A. Earhart,[§] Dileep D. Monie,[||] John J. Iandolo,[⊥] Patrick M. Schlievert,[||] and Douglas H. Ohlendorf*[,§]

Department of Biochemistry, Molecular Biology, and Biophysics and Department of Microbiology, University of Minnesota Medical School, Minneapolis, Minnesota 55455, and Department of Microbiology and Immunology, University of Oklahoma Health Sciences Center, Oklahoma City, Oklahoma 73190

Received March 29, 1999; Revised Manuscript Received May 24, 1999

ABSTRACT: The exfoliative toxins (ETs) cause staphylococcal scalded skin syndrome, a disease characterized by specific separation of layers of the skin. Evidence suggests that the toxins act as serine proteases, though the specific substrate and mode of action are not known for certain. The crystal structure of exfoliative toxin A (ETA) was reported earlier and shown to be similar to that of the chymotrypsin-like serine proteases. Here, we report the 2.4 Å resolution crystal structure of the other exfoliative toxin, ETB, which is 40% identical to ETA. The overall structures of ETA and ETB are similar including the positions of key residues within the active site. The structure of ETB supports the previous findings that the ETs are serine proteases that cleave substrates after glutamic acid residues. In this study we also discuss a number of structural differences including a large 14 residue loop insertion which may be a key feature involved in the differing biological properties of the ETs, particularly the pyrogenic and lethal activities of ETB not shared by ETA.

The human pathogen *Staphylococcus aureus* secretes a number of biologically relevant toxins. Among them, the exfoliative toxins (ETs),[1] serotypes A (ETA) and B (ETB), cause staphylococcal scalded skin syndrome (SSSS) (*1*). SSSS is characterized by specific separation of intraepidermal layers of the skin at the desmosomes. The illness usually affects newborns and can exfoliate 50% or more of the skin. Although peptide hydrolysis has never been demonstrated, the ETs do have an intrinsic albeit weak esterase activity with the substrate *N-tert*-butyloxycarbonyl-L-glutamic acid α-phenyl ester (Boc-GluOPh) (*2*). This enzyme activity is associated with skin exfoliation as mutations of putative catalytic residues abolish both esterase and skin exfoliation activities (*3*−*7*). The crystal structures of ETA (*6*, *7*) support earlier reports that the toxins are serine proteases; however, the mechanism by which they cause skin separation is still not clear.

The exfoliative toxins ETA and ETB are 40% identical to each other and 25% identical to the staphylococcal serine protease V8. ETA and ETB are 242 and 246 residues long, respectively, after their signal peptides are cleaved upon secretion. The reported p*I* values of ETA and ETB are 7.0 and 6.95 (*8*). The gene encoding ETA is located on the chromosome while the gene encoding ETB is found on a large plasmid.

Though controversial, early reports demonstrated that the ETs exhibit a mitogenic activity that is dependent on a particular variable region of the T-cell receptor (TCR) β chain (Vβ) leading to their classification as superantigens (*9*, *10*). Superantigens stimulate a subset of T-cells bearing specific Vβ regions on their TCRs, ultimately activating large numbers of T-cells by a mechanism unlike that of conventional antigens (*11*). Currently, there are many known superantigens including those from viral and bacterial origins. The prototypic and best studied family, the pyrogenic toxins (PTs), are grouped together based on a number of shared biological properties (*10*, *12*) and structural similarity. This family includes the staphylococcal enterotoxins (SEs), toxic shock syndrome toxin-1 (TSST-1), and the streptococcal pyrogenic exotoxins (SPEs).

Addressing the controversy surrounding the classification of ETs as superantigens, a thorough study by Monday et al. (13) reported that the ETs expanded Vβs 3, 12, 13.2, 14, 15, and 17. Curiously, the Vβ profiles of the ETs were similar to those of SEB and SEC (*13*, *14*). The earlier finding that

[†] Supported by NIH Grants AI 17474 (J.J.I.), HL 36611 (P.M.S.), and GM 54384 (D.H.O.).

[‡] Submitted to the Protein Data Bank under access code 1QTF.

* Corresponding author: Department of Biochemistry, Molecular Biology, and Biophysics, University of Minnesota Medical School, 4-225 Millard Hall, 435 Delaware St. SE, Minneapolis, MN 55455. Email: ohlen@dcmir.med.umn.edu.

[§] Department of Biochemistry, Molecular Biology, and Biophysics, University of Minnesota Medical School.

[||] Department of Microbiology, University of Minnesota Medical School.

[⊥] Department of Microbiology and Immunology, University of Oklahoma Health Sciences Center.

[1] Abbreviations: ETs, exfoliative toxins; ETA, exfoliative toxin A; ETB, exfoliative toxin B; SSSS, staphylococcal scalded skin syndrome; Boc-GluOPh, *N-tert*-butyloxycarbonyl-L-glutamic acid α-phenyl ester; TCR, T-cell receptor; Vβ, variable region of the β chain of the TCR; PTs, pyrogenic toxins; SEs, staphylococcal enterotoxins; TSST-1, toxic shock syndrome toxin-1; SPEs, streptococcal pyrogenic exotoxins; FC, flow cytometry; IEF, isoelectric focusing; HEPES, 4-(2-hydroxyethyl)-1-piperazineethanesulfonic acid; PDB, Protein database; MPD, 2-methyl-2,4-pentanediol; RMS, root-mean-square; DFP, diisopropyl phosphofluoridate; MHC, major histocompatibility complex.

10.1021/bi990721e CCC: $18.00
Published on Web 07/13/1999

Table 1: Summary of the Biological Properties of ETs

biological property	ETA	ETB	reference
skin exfoliation at specific site	+	+	(*1*)
cleaves ester Boc-GluOPH	+	+	(*2*)
inhibited by DFP	−	+	(*2*)
expands T-cells bearing Vβs 3, 12, 13. 2, 14, 15, and 17	+	+	(*13*)
expands T-cells bearing Vβ 20	+	−	(*13*)
corresponding reduction in surface TCR Vβs	+	−	(*13*)
induce fever (pyrogenic)	−	+	(*13*)
enhance susceptibility to endotoxin shock (lethal)	−	+	(*13*)

ETA stimulates V$\beta 2^+$ T-cells (*10*) was not supported by this report.

Monday et al. (*13*) also reported differences in the biological properties of ETs including expansion of Vβ20 by ETA but not by ETB. More significant was the finding that ETB unlike ETA was able to induce fever and enhance susceptibility to endotoxin shock in a rabbit model, properties shared by the PTs (*15*). Further, T-cells stimulated with ETB showed a corresponding population of T-cell receptors on their surface bearing the appropriate Vβ by flow cytometry (FC) analysis, while T-cells stimulated with ETA did not. Interestingly, ETA appeared to decrease the number of expected Vβ receptors on the surface of T-cells. The authors proposed that ETA may down-regulate T-cell receptors on the expanded set of T-cells, a process thought to occur for many superantigens (*11*). They further speculated that the biological differences observed for the ETs may derive from distinct signaling pathways, implying that different receptors or the same receptor with differing binding modes may be involved. See Table 1 for a summary of the various biological properties of the ETs.

Currently the ETs are the only structurally characterized examples of superantigens which also have an enzyme activity associated with them. The superantigenic activity of the ETs is independent of this enzyme function as the Ser 195(195) to Ala mutant form of ETA is enzymatically inactive, but retains mitogenic activity (*6*).

In this report we describe the crystal structure of exfoliative toxin B. The structure of this toxin is similar to ETA although there are key differences that may give insight into their dissimilar biological properties.

MATERIALS AND METHODS

Protein Purification. Exfoliative toxin B was purified from *Staphylococcus aureus* strain RN4220 containing *etb* from strain UT0007 (*16*). Bacteria were grown from a starter culture at 37 °C with aeration for 8 h in a dialyzed beef heart medium (*17*) containing chloramphenicol (10 μg/mL) and 1% glucose. After growth, the culture fluid and cells were treated with 4 volumes of absolute ethanol for 2 days to precipitate toxins. The precipitate was collected, suspended in 6 M urea, centrifuged to remove insoluble material (10000*g*, 30 min), and dialyzed 48 h at 4 °C against water. The dialysate was subjected to thin-layer isoelectric focusing (IEF), first in a pH 3.5−10 gradient and then in a pH 6−8 gradient. The toxin was dialyzed 2 days against 50 mM 4-(2-hydroxyethyl)-1-piperazineethanesulfonic acid (HEPES), pH 7.5, and then FPLC purified using a hydrophobic interaction column (Waters Chromatography, Milford, MA). The toxin eluted from the column as a single peak (as measured by the absorbance at $\lambda = 280$ nm) in a gradient from 1.7 to 0 M ammonium sulfate. The purified toxin was homogeneous on SDS−PAGE. Approximately 2 mg of pure protein was recovered per liter of culture fluid.

Table 2: Crystallographic Data Statistics

	ETB1
diffraction data	
space group	$C222_1$
cell dimensions	
a (Å)	69.97
b (Å)	71.09
c (Å)	108.37
mol./ASU	1
resolution (Å)[a]	15−2.4 (2.5−2.4)
redundancy	3.9 (2.7)
completeness (%)	94 (52)
I/σ	10.1 (1.03)
R-merge (%)[b]	5.6 (33)
unique reflections ($F > 0$)	10085
refinement (XPLOR) (*21*)	
no. of atoms	1935
R-factor (%)[c]	20.4 (33)
R_{free} (%)[d]	29.0 (45)
Ramachandran most favorable (%)	79
RMS deviation from ideal geometry	
bond length (Å)	0.012
bond angle (deg)	1.7
average *B*-factor (Å^2)	37.9
main chain	36.5
side chain	39.3
no. of water molecules	12

[a] Values in parentheses represent the last resolution shell (2.5−2.4 Å). [b] *R*-merge $= \sum_{hkl}\sum_i |I_i(hkl)_i - \langle I(hkl)\rangle|/\sum_{hkl}\sum_i I_i(hkl)$. [c] *R*-factor $= \sum||F_{calc}| - |F_{obs}||/\sum|F_{obs}|$. [d] 8% of the data which were used for the calculation of R_{free} were excluded from the refinement.

Structure Determination. Crystals of ETB were obtained in conditions similar to those reported earlier (*18*). Crystals were grown using the hanging drop method with 2 μL of well solution and 3 μL of protein solution (10 mg/mL). The best crystals grew in 25−30% 2-methyl-2,4-pentanediol (MPD) and 50 mM HEPES, pH 7.2−7.5, at 4 °C. Thin platelike crystals grew to a maximum size of 1 mm in 2 weeks.

Diffraction data were collected at room temperature on a Siemens area detector using monochromated Cu Kα radiation produced by a Rigaku RU-200B rotating anode and processed using the XENGEN software package (*19*). Data collection statistics are presented in Table 2.

The initial ETB model was created within the HOMOLOGY module of INSIGHT II (BioSym, La Jolla, CA) as described in Monday et al. (*13*) from ETA form IV (*6*). A single unambiguous orientation and translation solution of the ETB model was determined using AMORE in the CCP4 program suite (*20*). The initial *R*-factor after rigid body

Table 3: Flow Chart of the Purification of ETA and ETB

ETA/ L culture (2.0 mg)	ETB/ L culture (1.6 mg)	
↓	↓	
Ethanol precipitation (80% final volume) and resolubilization in distilled water	Ethanol precipitation (80% final volume) and resolubilization in distilled water	
↓	↙	↘
Water soluble fraction (2.0 mg)	Water soluble fraction (100 μg)	Water insoluble fraction (1.5 mg)
↓		↓
		Resolubilization in 6 M urea
		↓
		Soluble fraction (1.5 mg)
		↓
Dialysis against water and IEF in pH gradient of 3-10		Dialysis against water and IEF in pH gradient of 3-10
↓		↓
ETA pI 6.9 (1.8 mg)		ETB pI 6.9 (1.3 mg)

refinement was 45% using a resolution range of 15−2.8 Å. Refinement of the initial model by simulated annealing in X-PLOR (*21*), using data between 5 and 2.8 Å and $F > 2\sigma$, resulted in an *R*-factor of 34% and an *R*-free (8% removed) of 42%. Subsequent rounds of model building and refinement using positional and thermal parameter refinement including all data ($F > 0$) between 15 and 2.4 Å [bulk solvent correction included (*21*)], resulted in an *R*-factor of 23% and an *R*-free of 31%. Water molecules were added using the following criteria: $F_o - F_c$ density $>4\sigma$, reasonable $2F_o - F_c$ density $>1\sigma$, and within 3.4 Å of a hydrogen bond donor or acceptor. Further refinement and the addition of 12 water molecules resulted in a final *R*-factor of 20.4% and *R*-free of 29.0%. Two side chains [Arg 9(1K) and Gln 145(131)][2] of surface residues (refined as alanines) could not be modeled due to lack of $2F_o - F_c$ density. These side chains are included in the PDB file as common rotamers with occupancies of atoms beyond Cβ set to 0.

Visualization of the molecules and least-squares superimposition were done using O (*23*). Molecular surface calculations were made using GRASP (*24*). Model geometry was checked using PROCHECK (*25*).

RESULTS AND DISCUSSION

Purification of ETB. Purification of ETB in a manner similar to that used for ETA (*6*) consistently produced low yields of purified toxin. Only a small percentage of ETB was detected in the water-soluble fraction after ethanol precipitation (see Table 3). The water-insoluble toxin was readily resolubilized in 6 M urea. Urea was removed by dialysis against water for 2 days. The ability to resolublize the toxin in 0.01% Triton X-100 instead of urea suggested that ETB was not denatured. It is not known if ETB was insoluble in water due to its association with the bacterial membrane or another as yet unknown factor.

Structure of ETB. The final model includes all 246 residues of the ETB molecule with an *R*-factor of 20% and *R*-free of 29%. The ETB model has good geometry with 79% of the residues in the most favorable region of the Ramachandran plot and no residues in disallowed regions. ETB is similar to ETA [form IV, (*6*)] with a root-mean-square (RMS) deviation of 1.1 Å using 210 Cαs (see Figure 1 for a sequence alignment of the 2 toxins and Figure 2 for a Cα superimposition of ETA and ETB). The structural motif of the ETs is that of a chymotrypsin-like serine protease with two, six-strand β-barrels whose axes are roughly perpendicular (Figure 3). The active site of the molecule is located at the interface of the two barrels and includes an aspartic acid, a histidine, and a catalytic serine residue (see Figure 3 and Figure 4). ETB, like ETA and other members of the chymotrypsin serine protease family, has a C-terminal α-helix.

Similar to ETA and unlike the chymotrypsin-like family, ETB contains a distinct N-terminal domain. The domain includes an α-helix (αN) that lies adjacent to the C-terminal barrel domain near the base of the S1 binding site[3] (Figure 3). Helix αN is highly charged in both toxins with 8 of 15 residues in ETA and 6 of 11 residues in ETB being acidic or basic (Glu, Lys, or Arg). Based on sequence identity alone, the positions of the charged residues of helix αN were predicted to be conserved (*6*, *7*). The actual positions of the residues in the crystal structure of ETB are offset by three residues (or one turn) toward the carboxyl end of the helix (Figure 1). The loop connecting the N-terminal α-helix to the N-terminal β-barrel is three residues shorter in ETB [residues Phe 15(6)−Lys 22(16)] than in ETA [residues Tyr 17(6)−Lys 27(16)]. The shorter loop essentially leaves the tip of loop D[4] solvent-exposed in ETB [residues Tyr 159-(145)−Ser 160(151)], whereas in ETA residues His 165-(145) and Lys 166(146) are partially buried by Phe 25(12). The first residues of ETB [Lys 1(1C)−Tyr 3(1E)] contact residues of loop 3 [residues Glu 170(161)−Phe 172(163)] which differ from those of ETA whose N-terminal residues contact loop 2 [residues Leu 217(220)−His 221(223)]. Both loop 2 and loop 3 of ETB are four and three residues shorter, respectively, than their counterparts of ETA (Figure 2). Tyr 3(1E) of ETB forms part of a buried hydrophobic interface with residues Phe 172(163), Phe 178(184), and Leu 210-(225) of the C-terminal barrel domain as well as Ile 8(1J), Leu 11(2), and Phe 15(6) of the N-terminal helix. Tyr 3(1E) also forms a hydrogen bond with Glu 170(161). That the N-terminal helices of the ETs are unique and conserved suggests they may be important for biological function.

The Catalytic Site. The catalytic triad of the chymotrypsin-like serine proteases includes an aspartic acid, a histidine (both from the N-terminal barrel), and a catalytic serine residue (from the C-terminal barrel). Another conserved residue in this family is a serine residue which forms a hydrogen bond with the aspartic acid residue and is sometimes referred to as the fourth member of the catalytic triad (*29*). The catalytic sites of the ETs are similar to one

[2] Primary sequence numbers of the ETs refer to the linear sequence of the mature protein followed by topological equivalences of α-chymotrypsinogen in parentheses (6, 22).

[3] Substrate residues are represented by P*n*, ..., P2, P1, P1′, P2′, ..., P*n*′, where the bond is cleaved between P1−P1′, while S*n*, ..., S2, S1, S1′, S2′, ..., S*n*′ represents the corresponding binding sites on the protein following the convention of Schechter and Berger (27).

[4] Loops are named as described in Perona and Craik (28). Loop C is defined as residues 106(90)−115(103) in ETB and residues 112-(90)−121(103) in ETA; loop D is residues 155(141)−164(155) in ETB and residues 161(141)−170(155) in ETA; loop 2 is residues 206(218)−209(224) in ETB and residues 215(218)−222(224) in ETA; and loop 3 is residues 171(162)−175(181) in ETB and residues 177(162)−184-(181) in ETA.

```
     1A        1L       10        20    26   27        38         50           62A  63     70
     1                  20                  40                   60                  80
ETA: EVSAEEIKKHEEKWNKYYGVNAFNLPKELFSKVDEKDRQKYPYNTIGNVFVAGQTSATGVLIGKNTVLTNRHIAKFANG-DPSKVSFRPSINTDD
       <------αN------>          β-N  <αNa>       <βA1>   <-βB1>     β-C1 <-αA->         <--βD1-->
     1       10          20          30          40          50          60          70          80
ETB:   KEYSAEEIRKLKQKFEVPP---TDKELYTHIT--DNARSPYNSVGTVFVKGSTLATGVLIGKNTIVTNYHVAREAAK-NPSNIIFTPAQNRDA
         <----αN--->           β-N             <-βA1>   <--βB1-->  β-C1 <-αA->         <βD1>
V8 :                    VILPNNDRHQITDTTNGHYAPVTYIQVEAPTGTFIASGVVVGKDTLLTNKHVVDATHGDPHALKAFPSAINQD-

       75A   80A          92A100       110   111  118      128         140   151      160     180
          100                  120                 140                 160                 180
ETA: -NGNTETPYGEYEVKEILQEPFGAGVDLALIRLKPDQNGVSLGDKISPAKIGTSNDLKDGDKLELIGYPFDHKVNQMHRSEIELTTLSRGLRYY-
        <a>  βE1 <-b->          <βF1>                                  <-βA2->        <--βB2-->     β C2
     90        100        110        120        130        140        150        160        170
ETB: EKNEFPTPYGKFEAEEIKESPYGQGLDLAIIKLKPNEKGESAGDLIQPANIPDHIDIQKGDKYSLLGYPYNYSAYSLYQSQIEMFND---SQYF-
                  <βE1>          <βF1>                                  <-βA2>          <-βB2>       β C2
V8 : -----NYPNGGFTAEQITKY--SGEGDLAIVKFSPNEQNKHIGEVVKPATMSNNAETQVNQNITVTGYPGDKPVATMWESKGKITYL-KGEAMQY

      188    195     206                224                        233       243
                  200                 220                              240
ETA: -GFTVPGNSGSGIFNSNGELVGIHSSKVSHLDREHQINYGVGIG--------------NYVKRIINEKNE
                 βD2      <--βE2-->       <-βF2->                  <---αC--->
       180       190       200           210       220       230       240
ETB: -GYTEVGNSGSGIFNLKGELIGIHSGKGGQ----HNLPIGVFFNRKISSLYSVDNTFGDTLGNDLKKRAKLDK
                 βD2      <--βE2->        <-βF2>                   <---αC--->
V8 : DLSTTGGNSGSPVFNEKNEVIGIHWGGVPNEFNGAVINENVRNFLKQNIEDIHFANDDQPNNPDNP
```

FIGURE 1: Sequence alignment of ETA, ETB, and staphylococcal V8 protease. Sequential numbering of the ETs is above their respective sequences. Chymotrypsin numbering is above the sequential numbers of ETA. Secondary structural elements of ETA and ETB are indicated below their respective sequences. Underlined residues of ETB indicate structurally equivalent residues of the ETs.

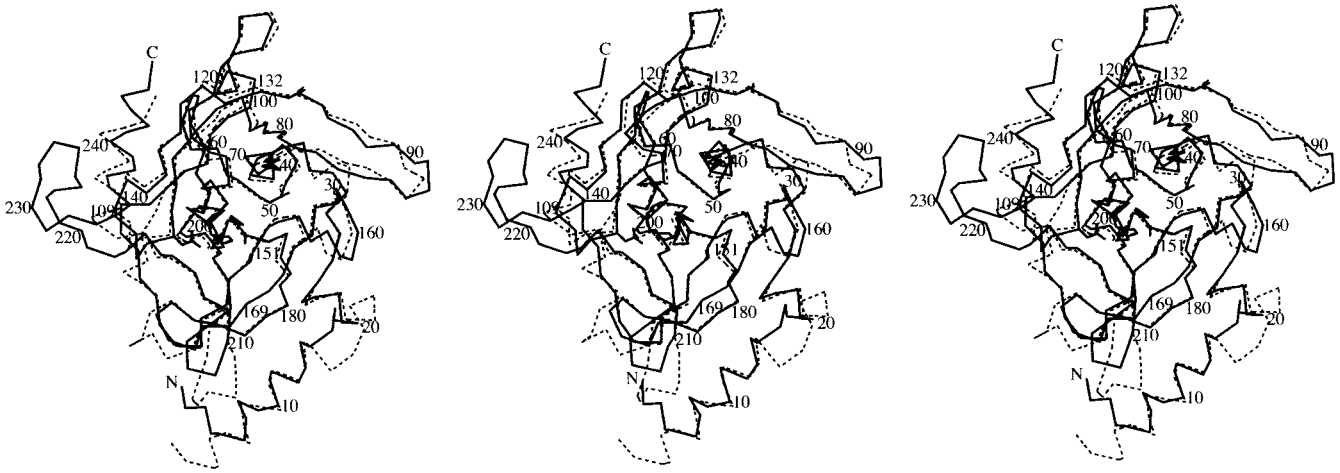

FIGURE 2: Cα comparison of superimposed ETA (dashed) and ETB (solid). Residue numbers are based on the linear sequence of ETB. This view represents the standard orientation except where noted. Stereo drawings show "wall-eye" stereo with the left two pair and "cross-eye" with the right two. Figures were prepared using SETOR (34) except where noted.

another and to those of this protease family, in general, with residues Asp 114(102), His 65(57), Ser 186(195), and Ser 202(214) of ETB aligning with those of ETA [Asp 120(102), His 72(57), Ser 195(195), and Ser 211(214), respectively] with an RMS deviation of 0.30 Å for all atoms (Figure 4).

The Occupied Oxyanion Hole. A notable similarity found in both ETs is the unique orientation of the peptide bond between Val 183(192) and Gly 184(193) [Pro 192(192) and Gly 193(193) in ETA] (Figure 4). This bond is flipped approximately 180° relative to other serine proteases for which structures are known (*22*). The carboxyl oxygen atom of Val 183(192) fills the oxyanion hole and forms hydrogen bonds to both the side chain oxygen (3.49 Å) and the main chain nitrogen (3.39 Å) of the catalytic serine residue [Ser 186(195)]. For ETA, the orientation of this peptide bond is further stabilized with a hydrogen bond between the main chain nitrogen of Gly 193(193) and the side chain of an aspartic acid residue Asp 164(144) in the adjacent loop (loop D). The peptide bond in ETB is not directly stabilized by a residue from loop D as the side chain of residue Asn 158-(144) is too far away (5.5 Å to nearest hydrogen bond acceptor). As a consequence of the occupied oxyanion holes, the crystal structures of the ETs represent inactive forms of the enzymes.

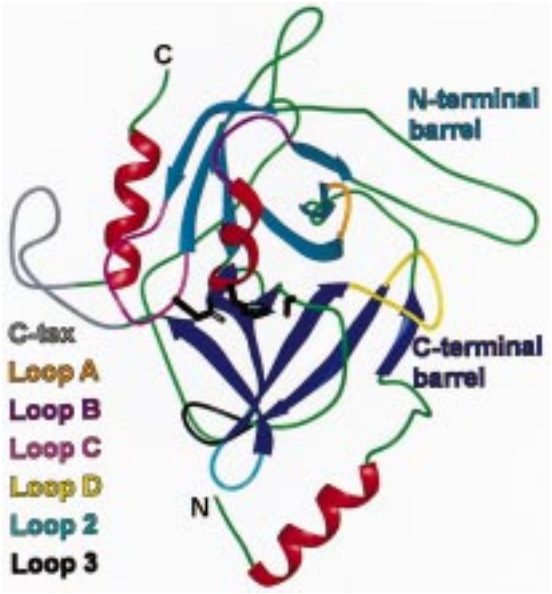

FIGURE 3: Secondary structure of ETB. α-Helices are red, β-strands of the C-terminal barrel are dark blue, and β-strands of the N-terminal barrel are light blue. Loops A, B, C, D, 2, and 3 are orange, dark purple, pink, yellow, cyan, and black, respectively. The C-terminal loop extension (C-tex) is gray. The side chains of Asp 114(102), His 65(57), and Ser 186(195) of the catalytic triad are black.

The reason Asn 158(144) is further away from Gly 184-(193) is due to a relatively large shift (>2 Å) of the residues at the tip of loop D [residues 157(143)−160(151]. This deviation from the analogous residues in ETA [Phe 163-(143) to Lys 166(151)] has its origin at Tyr 157(143) ($\phi = -89°$, $\psi = -9°$), which has a different side chain orientation ($\chi\ 1 = 70°$; *−gauche*) than the analogous residue Phe 163-(143) ($\chi\ 1 = -179°$; *trans*) in ETA ($\phi = -45°$, $\psi = -50°$). The side chain of Tyr 157(143) in ETB could easily adopt the *trans* orientation with a minor conformational change of loop D near Ala 161(152). In contrast, the phenylalanine of ETA could not adopt the *−gauche* position with the conformation of loop D as it would be less than 2 Å from Gly 193(193) and D164(144). As a consequence of the different conformation of loop D in ETB, Asn 158(144) is substantially further away from the active site, leaving only an interaction between the main chain nitrogen of Val 183-(192) and bulk solvent. The orientation of loop D in ETB is partially stabilized by two hydrogen bonds between the side chain of Glu 182(191) (OE1 and OE2) and the main chain nitrogens of Asn 158(144) ($d = 2.76$ Å) and Tyr 159(145) ($d = 3.17$ Å). A similar hydrogen bond is not present in ETA, as the analogous residue of Glu 182(191) is a valine [191(191)].

The orientation of loop D in ETB supports the hypothesis suggested by Vath et al. (*6*) that a conformational change of the loop likely accompanies activation of proteolysis in the ETs. The proximity of the loop to the active site not withstanding, a hydrogen bond acceptor must be available to stabilize the conformation of the peptide bond between Val 183(192) and Gly 184(193). This peptide bond is a key feature in the formation of the oxyanion hole and the stabilization of the tetrahedral intermediate which forms during catalysis (*30*).

An earlier study reported the esterolytic activity of ETA (with the substrate Boc-GluOPh) was partially reduced with the addition of the inhibitor diisopropyl phosphofluoridate (DFP), while the activity of ETB was completely inhibited (*2*). The different structural features of the ETs concerning the stabilization of the flipped peptide bond may help explain the different apparent activities toward the inhibitor. The additional stabilization of the flipped peptide bond by Asp 164(144) in ETA may increase the K_I of the inhibitor in comparison to ETB.

The S1 Binding Site. Proteases typically have high substrate specificities for the peptide or P1 residues after which they cleave. The S1 binding sites of the ETs suggest that the toxins have the ability to cleave peptide substrates after glutamic acid and possibly aspartic acid residues. In ETB, Lys 204(216) [Lys 213(216) in ETA] is in position to provide the countercharge to an acidic residue as suggested earlier with the report of the ETA structures (*6*, *7*). His 201-(213) and Thr 181(190) [His 210(213) and Thr 190(190) in ETA] would provide additional side chain contacts with a glutamic acid residue (Figure 4). Thus, the S1 binding sites of the ETs are highly conserved and indicate that they act upon similar substrates at this site.

A $+6\sigma$ feature in the $F_o - F_c$ map bridges the space between the side chain nitrogen of Lys 204(216) (2.50 Å) and the main chain oxygen of Gly 179(188) (2.55 Å) in ETB. This feature was modeled as a water molecule (Wat 102) and represents the only appreciable difference between the ETs with respect to the S1 binding site. The position of Wat 102 in ETB is occupied by the hydroxyl group of Tyr 18(7) of the N-terminal helix in ETA which bridges Gly 188(188) and Lys 216(213). Cavarelli et al. (*7*) reported that a deletion mutant of the first 20 amino acids of ETA (Δ1−20) completely inactivated the esterolytic and epidermolytic activities of the toxin. Given the proximity of the first 20 residues of ETA to the S1 binding site, particularly Tyr 18-(7), this result is not surprising. That a water molecule in ETB, however, can circumvent a direct interaction between Lys 204(216) and residues of the N-terminal helix suggests that indirect interactions between the two features play an important role in the function of the enzyme.

Sn−Sn′ Binding Sites. Beyond the P1 positions, proteases may also have preferences for residues up to five amino acids on either side of the scissile bond (P5 to P5′). While it is difficult to predict the substrate preferences of proteases outside the S1 binding site, especially without kinetic data, a comparison of the S*n*−S*n*′ sites of the ETs may provide insight into whether they cleave similar substrates outside the P1 position. Using the structure of trypsin complexed with bovine pancreatic trypsin inhibitor (*31*) as a model, the S5 to S2 binding sites of the ETs are not well-defined. This is due in part to the reduced lengths of loop 3 and loop C (Figure 3) of each toxin in comparison to other members of the family. In general, residues of loop 3 and loop C form the binding pockets that interact with amino acids in the P5−P2 positions (*28*). The ETs then do not appear to be very selective in their preference for any particular side chain on the N-terminal side of the scissile bond. Another interpretation is that the binding of a specific substrate may involve other as yet uncharacterized regions of the ETs.

The S1′−S3′ binding sites of this protease family generally involve residues of loop A, loop B (interacts with P1′ and

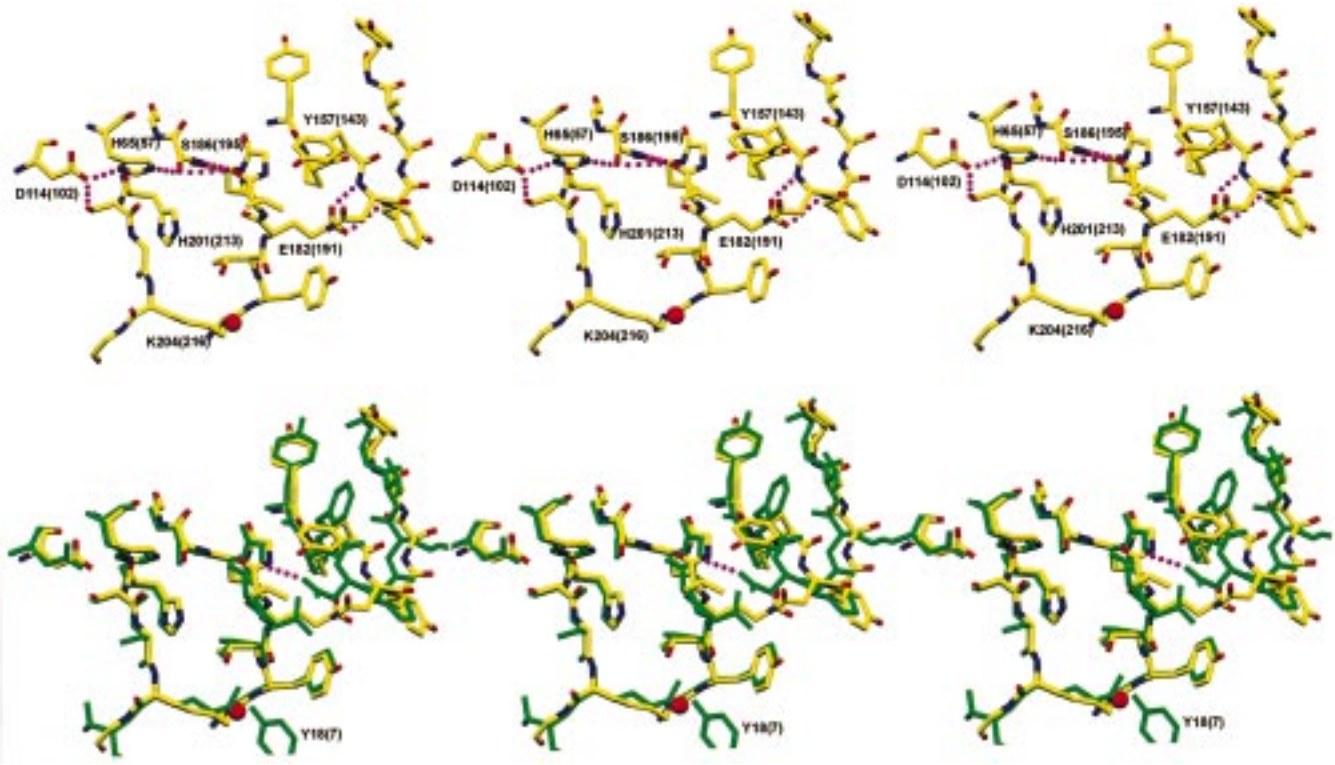

FIGURE 4: (Top) Active site of ETB. Carbon atoms are yellow, nitrogen atoms are blue, oxygen atoms are red, and select hydrogen bonds are magenta. Wat 102 is represented as a red sphere. Residue numbers are labeled as the single-letter amino acid code followed by the linear sequence number and chymotrypsin equivalencies in parentheses (see text). (Bottom) Superimposition of ETB and ETA (green).

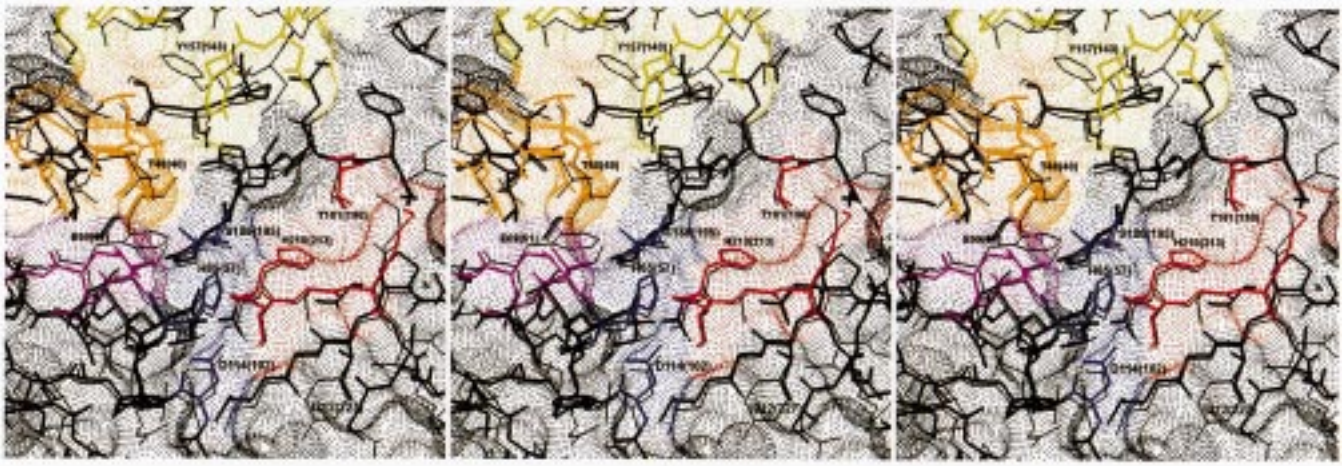

FIGURE 5: Connelly surface of ETB including the superimposed structures of ETB (thick lines) and ETA (thin black lines). The view is rotated 90° counterclockwise normal to the plane of the paper. Residues of the S1 binding site are red. Residues of the S1′ to S3′ sites are yellow (loop D), orange (loop A), and dark purple (loop B). Residues of ETB are labeled as in Figure 4. This figure was prepared using INSIGHT II (BioSym, La Jolla, CA).

P3′), and loop D (interacts with P2′)(Figure 5). The putative S1′ sites of the ETs are similar and somewhat hydrophobic with Thr 48(40), Ala 50(42), and Val 66(58) of ETB and Thr 55(40), Ala 57(42), and Ile 73(58) of ETA forming possible contacts. The slightly larger Ile 73(58) in ETA [versus Val 66(58) of ETB] is not likely to make a large difference in substrate binding affinity. Possible contacts of the S3′ sites differ between the two toxins and include Ser 47(39), Thr 48(40), and Glu 69(61) of ETB or Gln 54(39), Thr 55(40), and Phe 76(61) of ETA.

The S2′ sites of the ETs for the most part involve Tyr 157(143) of ETB and Phe 163(143) of ETA (Figures 4 and 5). As mentioned above, the orientations of these two residues are quite different between the two toxins. Tyr 157-(143) of ETB in its current position would not allow the binding of residues much larger than an alanine in the P2′ position. In ETA, the S2′ binding site is partially constricted by Asp 164(144) and Phe 163(143) but not nearly to the extent that it is in ETB by Tyr 157(143) alone. Consequently, a much larger side chain could potentially bind at this site in ETA. Another more intriguing interpretation is that the S2′ site of ETs is actually partially blocked by Tyr 157-(143) in ETB and to a lesser extent Phe 163(143) in ETA. This idea is consistent with the observation that the crystal structures of the ETs actually represent an inactive form of the enzymes. Blocking the substrate binding sites, including

the oxyanion hole by the unusual peptide flip as mentioned above, may be a mechanism by which the ETs reduce nonspecific binding of peptide substrates. Also consistent with this theory is the idea that a conformational change involving loop D including presumably Tyr 157(143) precedes activation (*6*). In consideration of these arguments, a comparison of the binding sites outside the S1 site of the ETs, particularly S2′, may be incomplete.

C-Terminal Loop Extension. The most apparent difference between the ETs is the addition of a large 14-residue loop [residues Arg 218(232A)−Gly 231(232N)] (C-tex) in ETB that connects the last β-strand of the C-terminal barrel (βF2) and the C-terminal helix (αC). A similar loop insertion has not been observed for any other member of this family of serine proteases. The C-tex loop makes numerous contacts with residues of the C-terminal helix [Leu 234(234)−Lys 243(243)], including a partially exposed salt bridge between Asp 227(232J) and Lys 240(240). Two ordered waters (Wat 103 and Wat 110) are buried by the C-tex loop. Wat 103 bridges Ser 225(232H) OG (3.08 Å) and Asp 232(232O) OD2 (2.80 Å) of the C-tex loop to Asp 237(232J) OD1 (2.75 Å) and Lys 240(240) NZ (3.39 Å) of the C-terminal helix. Wat 110 forms hydrogen bonds to Asp 232(232O) N (2.81 Å), Thr 229(232L) O (2.86 Å), and Ile 220(232C) O (3.12 Å). Other hydrogen bond interactions include Tyr 224(232G) O to Arg 241(241) NH2 (2.73 Å), Val 226(232L) N to Asp 237(237) OD1 (2.98 Å), Thr 229(232L) OG to Lys 240-(240) NZ (3.04 Å), and Asp 232(232O) OD1 to Asn 236-(236) ND (2.91 Å). Removal of the C-tex loop exposes a large hydrophobic patch that includes Ile 142(128), Ile 144-(130), Val 214(229), Phe 215(230), Phe 216(231), Tyr 109-(92A), Leu 113(101), Leu 115(103), Leu 234(234) and Leu 238(238).

In the crystal structure of ETB, the C-tex loop also forms part of a dimer interface with the C-terminal helix of a 2-fold related molecule (residues denoted with a prime) that buries 540 Å^2 of surface area. Val 226(232I) of the C-terminal loop extension and Leu 244(244) of the C-terminal helix form a small hydrophobic interface with the symmetry-related Val 226(232I)′ and Leu 244(244)′. Although the majority of the contact between the two symmetrical molecules is through van der Waals interactions, the side chain nitrogen (Nz) of Lys 246(246)′ forms three hydrogen bonds with the main chain oxygens of residues Ser 222(232E) (3.10 Å), Leu 223-(232F) (3.03 Å), and Ser 225(232H) (2.76 Å) of the loop extension. Although the function of the C-tex loop is unknown, it represents the largest structural difference between the ETs and may ultimately provide insight into the differing biological activities of ETA and ETB. It is also not known whether the dimer formation is biologically relevant or an artifact of crystal packing.

Glycine Binding Site. In ETA, a small molecule binding site was reported that was occupied by what was interpreted as a free glycine amino acid (*6*). This binding site is not apparent in ETB. Three residues of ETA reported to be in contact with the small ligand Lys 32(21), Arg38(26A), and Asn 91(71) do not have analogous residues in ETB. Further, residues Ala 82(69)−Pro 95(80) in ETB [residues Ser 89-(69)−Pro 101(80) in ETA] shift 2−3 Å in comparison to ETA, closing off what would be the ligand binding site and making it unlikely that a small ligand binds in this location of ETB. It is unknown whether a small ligand modulates any activity of the ETs; however, the glycine binding site of ETA not present in ETB may represent a difference that could explain the dissimilar biological properties of the ETs.

MHC and TCR Binding Sites. The ETs have been classified as superantigens based upon their ability to stimulate the proliferation of T-cells in a Vβ-dependent manner. Our current understanding of how superantigens activate T-cells implies that the ETs interact with major histocompatibility (MHC) class II molecules on an antigen-presenting cell and TCR on T-cells. The details of an interface between a superantigen and TCR have been published with the structure of the SEC3/TCR complex (*32*). The interface is relatively large (excludes 1300 Å^2 of solvent) and lacks charged residues as one may expect due to the large penalty of burying a charge. That the ETs have similar Vβ profiles and are structurally homologous suggests that the MHC and TCR binding sites of the toxins may be located in equivalent regions. That the ETs are only 40% identical (of which most identical residues are buried) suggests that binding modes of receptors have varying degrees of differences based upon residue interactions (backbone and side chain) of the ETs with the MHC and TCR.

While predicting the regions where MHC and TCR binding occurs on the ETs is not trivial, suggesting possible receptor sites may allow one to propose a rational approach to verify their location using site-directed mutagenesis. With the above considerations, possible receptor binding sites were located on the surface of the ETs based upon the following criteria: (1) A large surface area ($>$800 Å^2); (2) a surface area relatively devoid of surface charges; and (3) a similar placement in both ETs. Using similar criteria, a preliminary report, utilizing a homology model of ETB (*13*), located two possible TCR binding sites which are also consistent with the results presented here.

One site is located on the back (based upon the standard orientation in Figure 3) surface of the ETs. This site includes residues Ala 32(26B) to Asn37(28), Ile 55(47) to Gly 56-(48), and Ile 133(118) to Ile 138(123) in ETB [Gln 39(26B) to Asn 44(28), Ile 62(47) to Gly 63(48), and Ile 139(118) to Ile 144(123), respectively, in ETA]. The conformations of the backbone chain of these residues in the ETs are similar with an RMS deviation of 0.51 Å for all main chain atoms, including the Cβ carbons. The overall surface is somewhat similar between the ETs in this region with the largest difference being the side chains of Ser 34(26D), Gln 134-(119), and Asn 137(122) in ETB [Tyr 41(26D), Ser 140-(119), and Lys 143(122), respectively, in ETA]. Given the similarity of the backbone structures of the ETs, this site would be an example where differing side chain interactions alone could dictate differing binding modes of a receptor.

A second site proposed in the Monday et al. (*13*) study, although incorrectly modeled due to the unknown location of the 14-residue loop insertion, still fits the above criteria. This site is located adjacent to the catalytic triad (to the left side in Figure 3) and is the widest part of a large groove that originates at the interface of the two β-barrels near the catalytic site. The upper wall is formed by residues of loop C [Tyr 109(92A)−Leu 113(101) in ETB and Phe 115(92A)−Val 119(101) in ETA] and the base of the C-terminal helix. The lower wall is formed by loop 2 and loop 3 in both ETs. Interestingly, this site involves the C-terminal loop extension in ETB, which extends the upper wall of the groove. The

overall surface area of the groove is quite different between the ETs as this region represents the area where the backbone structures of ETA and ETB diverge the most (Figure 2). Although the surfaces are concave, access to the groove is partially blocked by the solvent-exposed side chain of Arg 218(232A) in ETB.

One other large area relatively devoid of surface charges in both ETs not mentioned in Monday et al. (*13*) is located near the N-terminal domain [residues Gln 13(4)−Thr 20-(14) in ETB and Asn 15(4)−Leu 25(14) in ETA] and loop D. This site also represents a region where the structures of the ETs differ considerably in conformation (Figure 2). It is unclear whether a divergence in structure as represented by the last two sites mentioned excludes them as potential receptor or TCR binding sites or whether the differences themselves allow the ETs to bind a receptor albeit with differing contacts. The latter as suggested in Monday et al. (*13*) may ultimately explain the differing biological properties of the ETs.

Conclusion. Consistent with the ETs functional similarities, the structures of ETA and ETB show a high degree of structural homology. The ETs appear to function as serine proteases, though it is not well understood why they do not exhibit peptidase activity in vitro. The oxyanion holes of both ETA and ETB are occupied, indicating the crystal structures represent an inactive form of the enzymes. The conserved S1 binding sites of the ETs suggest that they cleave substrates after glutamic acid residues although cleavage after aspartic acid residues cannot be ruled out. The ETs do not appear to have any preference for certain amino acids on the N-terminal side of the P1 residue. Whether the ETs have similar preferences for amino acids on the carboxyl side of P1 is unclear due primarily to the uncertainty of the conformation of loop D in the active form of the enzyme. The differing biological activities of the ETs, particularly the lethal and pyrogenic properties of ETB not shared by ETA, likely involve features that are not common between the toxins. The most apparent difference between the ETs is a 14-residue loop extension located before the C-terminal helix in ETB. This large loop is involved in a molecular dimer interface, although the biological relevance of this finding will need to be addressed further. Another potential feature that may be involved in the differing biological properties of the ETs is the small ligand binding site found in ETA but not ETB. Given the differing structural features on the surface of the ETs, the binding of separate receptors or the same receptor with differing binding modes likely explains the dissimilar functions of the ETs.

ACKNOWLEDGMENT

We acknowledge the Minnesota Supercomputer Institute for the use of computational resources.

REFERENCES

1. Melish, M. F., Glasgow, L. A., and Turner, M. D. (1972) *J. Infect. Dis. 125*, 129−140.
2. Bailey, C. J., and Redpath, M. B. (1992) *Biochem. J. 284*, 177−180.
3. Redpath, M. B., Foster, T. J., and Bailey, C. J. (1991) *FEMS Microbiol. Lett. 81*, 151−156.
4. Prevost, G., Rifai, S., Chaix, M. L., and Piemont, Y. (1991) *Infect. Immun. 59*, 3337−3339.
5. Prevost, G., Rifai, S., Chaix, M. L., Meyer, S., and Piemont, Y. (1992) in *Bacterial protein toxins* (Witholt, B., et al., Eds.) pp 488−489, Fischer, Stuttgart.
6. Vath, G. M., Earhart, C. A., Rago, J. V., Kim, M. H., Bohach, G. A., Schlievert, P. M., and Ohlendorf, D. H. (1997) *Biochemistry 36*, 1559−1566.
7. Cavarelli, J., Prevost, G., Bourguet, W., Moulinier, L., Delagoutte, B., Bilwes, A., Mourey, L., Rifai, S., Piemont, Y., and Moras, D. (1997) *Structure 5*, 813−824.
8. De Azavedo, C. S., Bailey, C. J., and Arbuthnott, J. P. (1988) *Methods. Enzymol. 165*, 32−36.
9. Morlock, B. A., Spero, L., and Johnson, A. D. (1980) *Infect. Immun. 30*, 381−384.
10. Marrack, P., and Kappler, J. (1990) *Science 248*, 705−711.
11. White, J., Herman, A., Pullen, A., Kubo, R., Kappler, J., and Marrack, P. (1989) *Cell 56*, 27−35.
12. Bohach, G. A., Fast, D. J., Nelson, R. D., and Schlievert, P. M. (1990) *Crit. Rev. Microbiol. 17*, 251−272.
13. Monday, S. R., Vath, G. M., Ferens, W. A., Deobald, C., Rago, J. V., Gahr, P. J., Monie, D. D., Iandolo, J. J., Chapes, S. K., Davis, W. C., Ohlendorf, D. H., Schlievert, P. M., and Bohach, G. A. (1999) *J. Immunol. 162*, 4550−4559.
14. Deringer, J. R., Ely, R. J., Stauffacher, C. V., and Bohack, G. A. (1997) *Infect. Immun. 65*, 4048−4054.
15. Kim, Y. B., and Watson, D. W. (1970) *J. Exp. Med. 131*, 611−628.
16. Jackson, M., and Iandolo, J. J. (1986) *J. Bacteriol. 166*, 574−580.
17. Blomster-Hautamaa, D. A., and Schlievert, P. M. (1988) *Methods Enzymol. 165*, 37−43.
18. Moras, D., Thierry, J. C., Cavarelli, J., and Piemont, Y. (1984) *J. Mol. Biol. 175*, 89−91.
19. Howard, A. J., Gilliland, G. L., Finzel, B. C., Poulos, T. L., Ohlendorf, D. H., and Salemme, F. R. (1987) *J. Appl. Crystallogr. 20*, 383−387.
20. Collaborative Computational Project, Number 4 (1994) *Acta Crystallogr. D50*, 760−763.
21. Brünger, A. T. (1990) *X-PLOR Version 3: A system for Crystallography and NMR*, Yale University Press, New Haven, CT.
22. Bode, W., Mayr, I., Baumann, U., Huber, R., Stone, S. R., and Hofsteenge, J. (1989) *EMBO J. 8*, 3467−3475.
23. Jones, A. T., Zou, J. Y., Cowan, S. W., and Kjeldgaard, M. (1991) *Acta Crystallogr. A47*, 110−119.
24. Nicholls, A., Sharp, K., and Honig, B. (1991) *Proteins: Struct., Funct., Genet. 11(4)*, 281−296.
25. Laskowski, R. A., MacArthur, M. W., Moss, D. S., and Thornton, J. M. (1993) *J. Appl. Crystallogr. 26*, 283−291.
26. Evans, S. V. (1993) *J. Mol. Graphics 11*, 134−138.
27. Perona, J. J., and Craik, C. S. (1995) *Protein Sci. 4*, 337−360.
28. Schechter, I., and Berger, A. (1968) *Biochem. Biophys. Res. Commun. 27*, 157−162.
29. McGrath, M. E., Vásquez, J. R., Craik, C. S., Yang, A. S., Hoing, B., and Fletterick, R. J. (1992) *Biochemistry 31*, 3059−3064.
30. Steitz, T. A., and Shulman, R. G. (1982) *Annu. Rev. Biophys. Bioeng. 11*, 419−444.
31. Marquart, M., Walter, J., Deisenhofer, J., Bode, W., and Huber, R. (1983) *Acta Crystallogr., Sect. B 39*, 480−488.
32. Fields, B. A., Malchiodi, E. L., Li, H., Ysern, X., Stauffacher, C. V., Schlievert, P. M., Karjalainen, S., and Mariuzza, R. A. (1996) *Nature 384*, 188−192.

BI990721E